Journal of Forensic Biomechanics

Hamedani and Navidbakhsh, J Forensic Biomed 2015, 6:2
DOI: 10.4172/2090-2697.1000122

Research Article Open Access

Blood Flow Pattern in Bending Coronaries in Coronary Artery Bypass Grafts

Borhan Alhosseini Hamedani[1*] and Mahdi Navidbakhsh[2]

[1]Parks College of Engineering, Aviation and Technology, Saint Louis University, St. Louis, Missouri, USA
[2]School of Mechanical Engineering, Iran University of Science and Technology, Tehran, Iran

Abstract

This study investigates the effect of coronary bending in a 3D model of a Coronary Artery Bypass Graft (CABG), while considering Fluid-Structure Interaction (FSI). The coronary had an axisymmetric stenosis with lumen reduction of 65% and the arterial wall was modeled as linear elastic. The blood was considered a Newtonian fluid and pulsatile pressure was applied as the boundary condition for the two inlets and the outlet. Results revealed that the bending led to a lower level of coronary flows, but higher graft flows. Compared to the straight coronary model, Shear Stress (SS) in the outer wall of the stenosis in the curved model increased by 9%. For both models, there was a recirculation area downstream of the stenosis in which Wall Shear Stress (WSS) was low, which might put this region at high risk of restenosis. For the bending model, this area expanded in the inner wall while contracting in the outer wall. For both models, wall effective stress increased near the anastomosis area, especially at the heel of the graft, while the bending model did not alter this stress along both vessels.

Keywords: Coronary artery bypass graft; Fluid structure interaction; Pulsatile pressure; Coronary artery; Wall shear stress; Maximum effective stress

Introduction

Cardiovascular Disease (CVD) is the main cause of mortality in developed countries. According to the American Heart Association (AHA), more than 81 million patients were diagnosed with one or more types of CVD in the U.S in 2006 and the mortality was 831,300 [1]. Among different types, Coronary Artery Disease (CAD) imposed the greatest threat with a 51% mortality rate and $96 billion in treatment costs, directly or indirectly, and it was introduced as the largest major killer of Americans, with 425, 425 losses.

In atherosclerosis disease, the lumen area reduces and consequently sufficient amount of blood is no supplied to the myocardium. The mechanism of plaque formation and therefore, lumen area reduction is known, and hemodynamics plays a crucial role in it [2]. Wall Shear Stress (WSS) and Wall Shear Stress Gradient (WSSG) are the two important parameters that affect the response of endothelial cells; in Shear Stress (SS) lower than 0:4(Pa) the orientation of these cells change so that the chance of Low Density Lipoprotein (LDL) sedimentation raises, which throughout a complicated process, results in the development of stenosis [3]. On the other hand, there is a high risk of endothelial cell and red blood cell rupture at SS greater than 42(Pa) [4] And 150(Pa) [5] respectively. However, these parameters are not experimentally measurable in small diameter arteries [6,7]. To investigate blood flows pattern in arteries and its parameters such as WSS and WSSG, Computational Fluid Dynamics (CFD) is a non-invasive, appropriate technique [6,7]. More realistic geometries and appropriate boundary conditions are the key factors to achieve results that are more reliable. Since the 70s, many researchers have employed CFD in different geometries and boundary conditions to simulate blood flows in the arteries with various assumptions and simplifications such as 2D flows, steady state flows, rigid walls and Newtonian viscosity. Caro [8] explained the relationship between SS and atherosclerosis. Ahmed and Gidden considered pulsatile blood flows in a stenosis model [9]. For a 2D end to side anastomosis, Pietrabissa [10] simulated steady state flows in an aorta-coronary bypass, and Inzolli [11] developed a 3D model of aorta-coronary bypass with steady state flows. Bertolotti and Deplano [12] simulated a 3D steady model of flows for a coronary bypass and observed post-stenotic flows patterns; they considered rigid walls in a 3D coronary in a straight geometry for both host artery and graft with velocity inlet boundary condition. Guo et al. [13] mentioned that placement of the graft immediately after the stenosis results in a better patency of grafts. Boutsianis [14] reconstructed a 3D realistic porcine coronary artery including its branches. Sankaranarayan et al. [7] investigated the effect of a 3D aorta-coronary bypass with a larger diameter of graft and pointed out that WSS in the graft bed changed noticeably with larger grafts. In order to develop more realistic models, the effect of vessel deformation on the pattern of blood flows has recently been considered with fluid-structure interaction (FSI) models. Tang et al. developed patient-specific models of stenosed carotid [15] and coronary [16] artery based on reconstructed images from MRI with pulsatile pressures for boundary conditions and considering FSI. They also examined the mechanical properties of fibrous tissues, lipid and intact coronary arteries to consider a non-isotropic artery model [17]. Holzapfel et al. investigated the mechanics of arteries in a multilayer model, which considered the presence of collagen. They validated their model, known as Holzapfel-Ogden, with experimental results from mechanical tests on arteries [18-20]. Valencia et al. [21] and Li et al. [22] studied WSS variation for an axisymmetric stenosis in different degrees of stenosis. Mohammadi and Bahramian [23] compared two conventional boundary conditions in simulation of a stenosed coronary artery: velocity and pressure boundary conditions. They concluded that the former boundary condition cannot lead to results compatible with the human physiology.

***Corresponding author:** Borhan Alhosseini Hamedani, Parks College of Engineering, Aviation and Technology, Saint Louis University, St. Louis, Missouri, USA, Tel: 3146622371; E-mail: alhosseinihamed@slu.edu

Received May 22, 2015; **Accepted** July 03, 2015; **Published** July 10, 2015

Citation: Hamedani BA, Navidbakhsh M (2015) Blood Flow Pattern in Bending Coronaries in Coronary Artery Bypass Grafts. J Forensic Biomed 4: 122. doi: 10.4172/2090-2697.1000122

In spite of the valuable studies in simulation of stenosed arteries and CABG, a 3D model of CABG considering FSI and pulsatile pressure was not found in the literature. Furthermore, there was little insight on the effectiveness of a small diameter bypass. Therefore, the aim of this study is to apply a more realistic boundary condition to a 3D model of CABG with a small caliber bypass. The primary study was previously presented in a conference [24] and the model was developed further with a curved coronary artery to compare the result of bending of the coronary artery due to the heart beating.

Materials and Methods

Geometric model

The coronary model was developed with an axisymmetric stenosis with 65% lumen reduction as shown in Figure 1. The coronary diameter (D) was assumed to be 4 (mm) and the total length 120 (mm), which equals to 30D. The bypass artery diameter was 0.5D and the curvature radius for the curved coronary model was 25D. Wall thickness in both host and graft arteries were 0.5(mm) and the graft angle was 30° at the anastomosis location. The stenosis was 12.5D downstream of the coronary inlet and the graft location was 6.25D distal to the stenosis.

Fluid domain

Blood was assumed as a Newtonian, incompressible fluid with a density of ρ=1050 (kg=m^3) and a dynamic viscosity of σ = 0:00345(Pa.s). Because of the movement of the boundaries, the incompressible momentum equations were solved using an arbitrary-Lagrangian-Eulerian (ALE) configuration with the governing equations as follows:

Continuity equation:

$$\nabla \cdot \vec{V_f} = 0$$

Momentum equation for the fluid domain:

$$\rho\left[\frac{\partial \vec{V_f}}{\partial t} + \left(\left(\vec{V_f} - \vec{V_s}\right)\cdot\nabla\right)\vec{V_f}\right] = -\nabla \cdot P + \nabla \cdot \tau$$

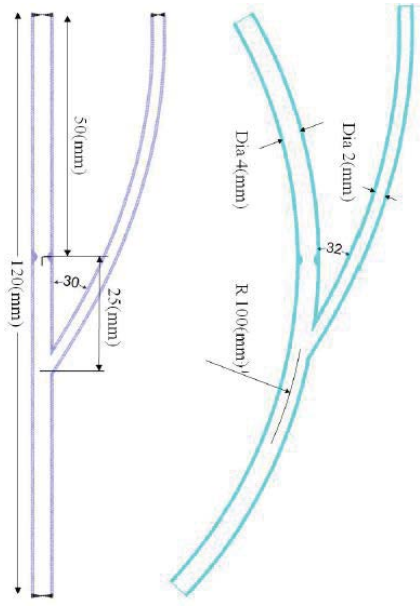

Figure 1: Geometry of the two bypass models.

Where ρ indicates the fluid density, $\vec{V}$ is the velocity vector, P and $\mathbf{T}$ are the pressure and deviatoric stress tensors, respectively. Subscripts f, s represents fluid and solid domains, respectively. Thus, $(\vec{Vf} - \vec{V}s)$ blood relative velocity with respect to the moving arterial wall [21].

Solid domain

Both arterial and graft walls were considered as a linear elastic, incompressible and homogenous material with a Poissons ratio of $^{\upsilon}$ = 0:49 and a density of ρ= 1060(kg=m^3), but with different stiffness namely Young modulus of E= 1(MPa) and E= 0:7(MPa) for the coronary artery and the graft, respectively. Considering the tensor of elasticity for a linear material, the stress-strain relationship is:

$$\vec{\sigma} = E\vec{\epsilon}$$

Where E is the fourth-order elastic tensor and $\vec{\sigma}$ and $\vec{\epsilon}$ are the stress and strain vectors, respectively [22]. Momentum equation for the solid domain with Lagrangian formulation is:

$$\rho_s \frac{\partial^2 d_i}{\partial t^2} = \frac{\partial \sigma_{ij}}{\partial x_i} + F_i \quad i = 1,2,3$$

Where d_i and σ_{ij} are the components of the displacements and stress tensors, ρs is the arterial wall density and Fi represents the body forces acting on the solid domain [22].

Coupled model

In the common boundaries between the fluid and solid domains, displacement, velocity and stress are the same:

$$\vec{d_s} = \vec{d_f}$$

$$\sigma_s \cdot \vec{n_s} = \sigma_f \cdot \vec{n_f}$$

$$\vec{V_s} = \vec{V_f}$$

Where d is the displacement, $\vec{n}$ is the boundary normal vector and σstand for the stress tensor [21].

Boundary conditions

Pulsatile pressure as demonstrated in Figure 2 was used in the fluid domain as the boundary condition for the both inlets and the outlet. These pressures were obtained from Tang et al.'s study on simulation of a stenosed coronary [16]. In the solid domain, the two ends of the coronary model as well as the inlet of the graft were fixed in all directions. Furthermore, the symmetric plane of the model was confined to eliminate any vibration in the model. Finally, the common boundary between the fluid and solid domains was defined as an FSI boundary.

Numerical model

The coupled model of the fluid and solid domains was solved with the commercial finite element package ADINA (v8.5, ADINA R&D, Inc., Cambridge, MA) using 3D tetrahedral elements for both domains.

Large displacement and small strain formulation was applied for the solution and the governing finite element equations were solved with the Newton-Raphson iteration method. In order to avoid the divergence of the solution, both pressures were increased in 10 increments of 0:1(s), then they remained constant for 5 time intervals of 0:01(s) to attenuate the transient effects. Finally, 95 time increments of 0:01(s) was used to complete the solution. Therefore, the total time of solution was 2(s). Sparse solver was used for the iterations and the residual tolerances for all degrees of freedom were set to 0:001.

Grid resolution study

To achieve a smoother mesh and to control the grids more precisely, the fluid domain was divided into 6 sub-domains, which were linked together using \Face-link" as demonstrated in Figure 3. The proper refinement of the mesh near the walls and the high gradient regions was easier when applying this approach. In the solid domain, because of the small thickness of the arterial wall, only the elements near the stenosis and the graft anastomosis were refined. ADINA suggests studying each domain separately, and then combining both domains [25]. The implementation of this method helped achieve a suitable grid resolution faster. To study the solid domain, the inlet pulsatile pressure was applied to the model. Since the greatest pressure occurred at t= 1:38(s), the maximum effective stress at this time was compared for each grid as depicted in Table 1. The difference between the model with 148,000 elements and 278,000 elements was only 2%, and the former grid was selected for the solid domain. For the fluid domain, the straight coronary model was studied considering rigid walls. WSS and maximum velocity were compared for each grid resolution. The results were accurate enough for 296,000 elements, with less than 5% change in WSS and 2.5% change in maximum velocity as indicated in Table 1. Having combined both solid and fluid domains, based on obtained insight in these domains, we could investigate each domain faster and easier, whereas in similar studies several grid studies have been performed to obtain an acceptable grid resolution [15]. A quad-core, 3.50GHz processor with 8 GB of RAM memory was used on a 64bit Windows 7 Operating System and the iterations took approximately 16-18 CPU hours.

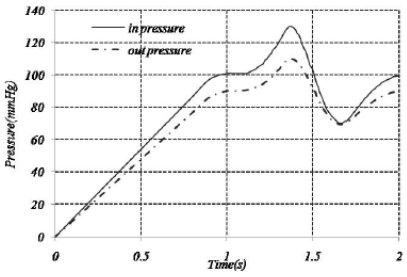

Figure 2: Inlet and outlet pressures.

Figure 3: Mesh refinement near the stenosis.

Solid Domain		Fluid Domain		
No. of elements	Maximum Effective Stress (Pa)	No. Of elements	Maximum Velocity(m/s)	WSS(Pa)
49,300	15900	-	-	-
75,000	13800	213000	1.09	35.8
14800	128400	296000	1.16	40.2
27800	12600	350000	1.19	42.2

Table 1: Grid study of the solid and fluid domains.

In order to evaluate the accuracy of the outcomes, two extra models of the straight coronary with 50% and 80% stenosis were developed to compare the results with those obtained by Valencia et al. [21] who studied an axisymmetric stenosis with 50%, 60% and 70% lumen area reduction. The stenosis model and flows rate in their model was the most comparable model that was found in the literature and they considered FSI for their simulations. The WSS for normalized velocity was compared between the two studies as depicted in Figure 4 and the results were in very good agreement. Furthermore, the results of the effective stress near the graft were compared with those obtained by Holzapfel et al. [26]. The applied pressure in the current study was the same as their model and they studied the stresses near the graft location in a graft with similar anastomosis angle. Again, the values of effective stress in both studies were in good agreement in both models with greater values near the heel of the graft.

Results

In this study, the first second of the simulation (0-1(s)) was a linear rise in the inlet and outlet pressures in order to adapt the pressure and obtain a converged solution. Therefore, the results are prepared for 1-2(s).

Blood flows within a cycle

With the linear increase in the pressure difference between the inlets and the outlet, blood flows rate in both the coronary artery and the bypass graft increased, albeit non-linearly Figure 5, 0-1(s). However, Poiseuille equation presents a linear relationship between the flows rate and pressure difference ($\Delta P = 8\mu LQ = (\pi r^4)$) Maximum and minimum flows rates occurred at t= 1:38(s) and t= 1:7(s), respectively, and Figure 5 depicts the flows rate versus time for the graft and coronary arteries in two models.

The average outflows of the straight coronary within a cycle was 2.8(ml=s). Compared to the coronary artery, the grafts in both models could not deliver sufficient amount of blood. For the straight coronary model, the average bypass flows was 0.47(ml=s) which was 16.9% of the total outflows. The coronary bending resulted in a 7.5% reduction in the coronary flows, and a 4.8% increase in the bypass flows. Yet, the

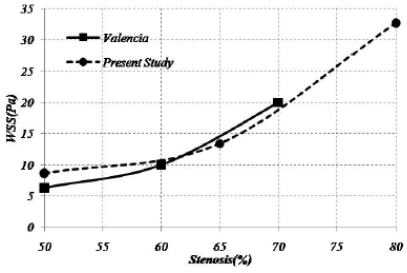

Figure 4: Average WSS in the current study and Valencia's study.

overall flows dropped by 4% compared to the straight model (Figure 5).

Velocity vectors and recirculation area

Before the stenosis, the velocity profile was axially symmetric along the straight coronary model while the flows skewed towards the outer wall in the bending model. Figure 6 presents the velocity profiles at t= 1:38(s) in the curved coronary model. Near the stenosis, the profile was jet-shaped. Maximum velocity in the jet increased from 1:1(m=s) in the straight coronary to 1:17(m=s) in the curved model. Further downstream, near the anastomosis, the coronary flows skewed towards the bed of the graft in both models. There was a vortex region downstream of the stenosis as shown in Figure 7. In this region, the blood velocity was lower than that of the intact areas. This recirculation area was almost symmetric for the straight coronary, whereas the curved model had a smaller recirculation area with a shorter reattachment point in the outer wall, and a larger recirculation area with a longer reattachment point in the inner wall as illustrated in Figure 7(a,b).

The cross sectional view of the velocity vectors revealed that the vortices after the stenosis had 3D structures, and in spite of an axisymmetric stenosis the flows pattern was not axisymmetric. For both the straight and curved models, there were two major, counter-rotating recirculation regions in the upper wall and lower wall of the artery which is evident in Figure 8 1.2(mm) downstream of the center of the stenosis for both models. Each of these recirculation areas separated into two smaller regions (left and right) in both models.

In addition, the recirculation area developed as the flows rate increased as demonstrated in Figure 9 near the graft at t =1:38(s) and t=1:7(s) for the maximum and minimum flows rates, respectively. The length of the vortex increased from 2:5(mm) to 3:5(mm) and its height reached the stenosis height. The separation point in all cases occurred in the back side of the stenosis.

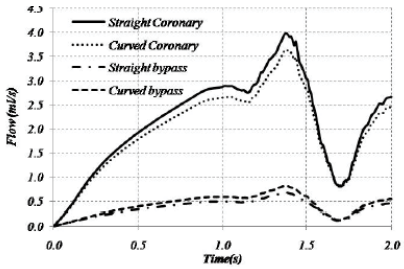

Figure 5: Flow of the coronary and graft in two models.

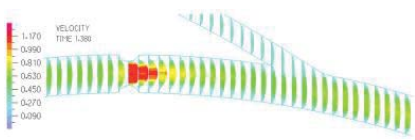

Figure 6: Velocity profile in the bending coronary model.

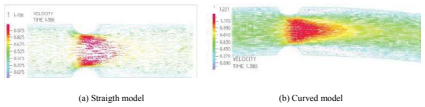

Figure 7: Recirculation area near the stenosis.

Wall shear stress

WSS was almost constant along the coronary before the stenosis as demonstrated in Figure 10. Near the stenosis, WSS decreased slightly and then increased over the stenosis with maximum WSS occurring at the front side. The non-symmetric recirculation region was more clearly evident in this figure. Near the graft, the two flows merged together resulting in a higher WSS at the toe and the bed of the graft. Similar to the flows rate, there was a non-linear correlation between the pressure rise and WSS. Maximum WSS for the straight coronary was 25:2(Pa) on average, which increased by 9% (to 27:5(Pa)) for the curved model as demonstrated in Figure 11.

In order to obtain a better insight into different locations of the model, 7 arbitrary points were selected in the bending coronary model. The straight model had similar results, except at the inner side and outer side of the stenosis. The first point was at the tip of the inner stenosis (Inner wall). The second point was at the opposite side, at the outer stenosis (Outer wall). The third point was at the recirculation area, 0.1(mm) after the stenosis (Recirculation). The fourth and the fifth points were at the heel and the toe of the graft, respectively. Finally, the sixth (Intact coronary) and the seventh (graft) points were selected at the outer wall of the coronary and bypass arteries, respectively.

The inner wall of the stenosis experienced lower SS than the outer wall as depicted in Figure 12. In the inner vortex the SS was half of that in the normal location, yet had a negative value. WSS in the intact area of the coronary and graft was practically the same with an average of 3:6(Pa). In the graft region, WSS increased by 25% near the toe of the graft (4:5(Pa) on average) while decreasing slightly in the heel.

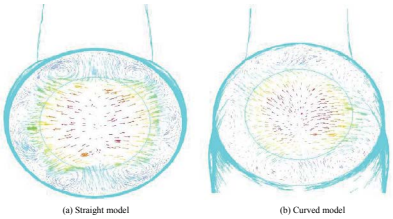

Figure 8: Recirculation area near the stenosis in a cross sectional view.

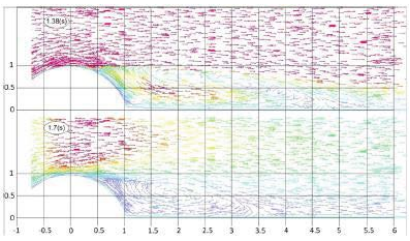

Figure 9: Recirculation area at time t = 1:38(s) and t = 1:7(s).

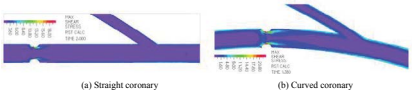

Figure 10: WSS along the vessels at t = 1:38(s).

Maximum effective stress and wall displacement

Although the key parameters in plaque rupture have yet to be specified clearly, it is hypothesized that maximum effective stress is one of the possible factors [7,8]. This stress followed a linear correlation with the pressure rise. The stenosis experienced slightly lower stress than that of the intact area and the bending did not affect the stress pattern noticeably. However, effective stress increased dramatically near the anastomosis in both of the models, with the highest values at the heel as depicted in Figure 13. These figures are presented in different scales in order to capture further details. Maximum effective stress at the tip of the stenosis and heel of the graft is compared in Figure 14 for the straight coronary model. Evidently, the heel of the graft had more than 6 times the stress compared to that of the intact area, with 325(KPa) on average. Likewise, the wall displacement had a linear correlation with pressure rise with average and maximum wall displacements of 0:08(mm) and 0:11(mm), respectively, which equaled to 5:5% average strain.

Discussion

The investigation of the effect of a small diameter bypass graft, and the coronary bending in a 3D CABG model was the main aim of the present study. The consideration of FSI formulation results in a more realistic model of CABG since the arteries expand due to the pulsatile pressure. Furthermore, an FSI study provides information on the solid domain such as wall effective stress, which is not obtainable in a CFD simulation with rigid walls. Breaking the model into subdomains and linking them together facilitated the control of the mesh quality. In addition, the separate study of the grids in each domain helped achievement of an appropriate grid density faster. Tang et al. employed this method to simulate the flows in a stenosed carotid [15] and coronary [17] with pulsatile flows. The small diameter graft did not provide noticeable flows compared to the stenosed coronary in both models. Therefore, in order to recover the decreased flows, a larger graft is required. Furthermore, FSI simulations showed that bending noticeably altered the flows pattern. Due to the bending, the coronary flows and overall flows decreased, while the graft flows increased slightly. Near the graft in both models, the flows skewed towards the bed of the graft, and WSS increased slightly in this location. Such an increase might result in intimal hyperplasia at this location. The stenosis engendered a recirculation area. This region was not symmetric in the straight model even if the geometry was symmetrical. Bluestein [27] and Valencia [21] pointed out this non-symmetric pattern in their studies. Coronary bending resulted in a larger region in the inner wall and a smaller region in the outer wall. These regions had lower velocities and SS in both models. Since orientation of endothelial cells is directly influenced by SS [3,6], the risk of LDL sedimentation might increase, which might lead to restenosis downstream of the stenosis. Furthermore, maximum WSS in both models were lower than the critical values to damage the haemoglobin or endothelial cells. However, further development of the disease, or higher physical activities might result in the initiation of the damage. Maximum effective stress near the graft was higher than the stenosed or the intact area with more than 6 times greater values at the heel of the graft. Cacho and Holzapfel [26] emphasized these higher stresses near the anastomosis for a multilayer aorta coronary bypass. These higher stresses might put this region at a high risk of rupture and further attention might be needed at this region while attaching the graft artery to the host artery. In an in vivo model, the effect of sutures and local inconsistencies might increase these stresses and the risk of rupture at this region. Finally, considering the deformation of the vessels, maximum radial strain was 5:5%, which is in accordance with McDonald's study that reported a 5% maximum radial strain in major arteries [28].

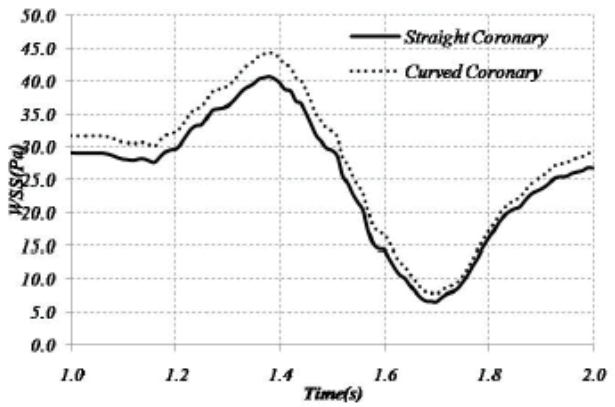

Figure 11: Maximum WSS on the stenosis.

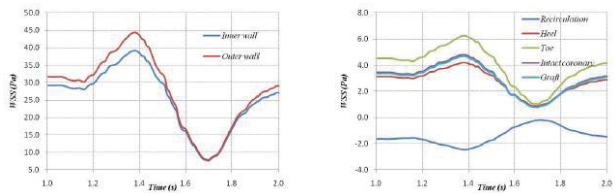

Figure 12: WSS at different locations in the bending coronary model.stenosis.

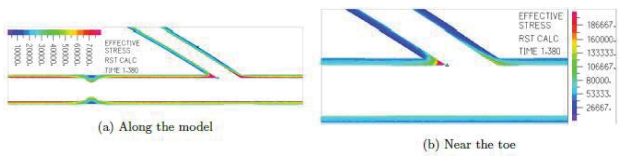

Figure 13: Maximum effective stress in the straight coronary model t = 1:38(s).

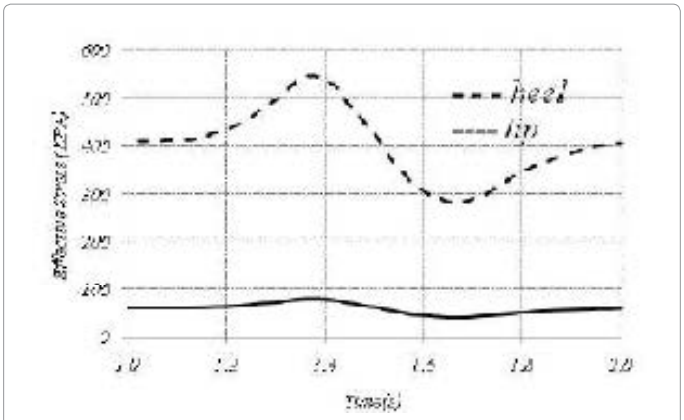

Figure 14: Maximum effective stress at the tip of the stenosis and heel of the graft in the straight model.

Limitations of the Study

Although the outcomes of this study were consistent with other

similar studies, it did not include an experimental measurement to evaluate the credibility of the outcomes. Furthermore, the blood vessels as well as the stenosis were assumed as a linear elastic material, while soft tissues represent non-linear mechanical behavior. Due to this assumption, maximum effective stress at the stenosis was lower than that of the intact area which might not be a credible outcome. Finally, the effect of the surrounding tissue was not considered in this model. In fact, the coronary artery is surrounded by myocardium and the lumen area might decrease due to beating.

Convict of Interest Statement

The authors declare that there is no convict of interest regarding the publication of this paper.

References

1. Lloyd-Jones (2010) Erratum: Heart disease and stroke statistics-2010 update: A report from the american heart association. Circulation 121: e46-e215.
2. Ross R (1999) Atherosclerosis-an inammatory disease. N Engl J Med 340:115-126.
3. Cunningham KS, Gotlieb AI (2005) The role of shear stress in the pathogenesis of atherosclerosis. Lab Invest 85: 9-23.
4. Valenta J (1993) Biomechanics Clinical Aspects of Biomedicine Series. Elsevier Science Limited.
5. Liu B. (2007) The influences of stenosis on the downstream flow pattern in curved arteries. Medical Engineering & Physics 29: 868-876.
6. Santos, Dos JAPP (2009) The influence of geometric factors on the wall shear stress distribution in realistic human coronary arteries.
7. Sankaranarayanan M, Chua LP, Ghista DN, Tan YS (2005) Computational model of blood flow in the aorto-coronary bypass graft. Biomed Eng Online 4: 14.
8. Caro CG, Fitz-Gerald JM, Schroter RC (1969) Arterial wall shear and distribution of early atheroma in man. Nature, 223: 1159-1161.
9. Ahmed S, Giddens D (1984) Pulsatile poststenotic ow studies with laser doppler anemometry. J Biomech 17: 695-705.
10. Pietrabissa R, Inzoli F, Fumero R (1990) Simulation study of the fluid dynamics of aorto-coronary bypass. J Biomed Eng 12: 419-424.
11. Inzoli F, Migliavacca F, Pennati G (1996) Numerical analysis of steady flow in aorto-coronary bypass 3-d model. Journal of Biomechanical Engineering, 118: 172-179.
12. Bertolotti C, Deplano V (2000) Three-dimensional numerical simulations of flow through a stenosed coronary bypass. J Biomech 33: 1011-1022.
13. Guo LR, Steinman DA, Moon BC, Wan WK, Millsap RJ (2001) Effect of distal graft anastomosis site on retrograde perfusion and flow patterns of native coronary vasculature. Ann Thorac Surg 72: 782-787.
14. Boutsianis E, Dave H, Frauenfelder T, Poulikakos D, Wildermuth S, et al. (2004) Computational simulation of intracoronary flow based on real coronary geometry. Eur J Cardiothorac Surg 26: 248-256.
15. Tang D, Yang C, Zheng J, Woodard P, Sicard G, et al. (2004) 3d MRI-based multicomponent FSI models for atherosclerotic plaques. Ann Biomed Eng 32: 947-960.
16. Tang D, Yang C, Kobayashi S, Zheng J, Woodard P, et al. (2009) 3d MRI-based anisotropic FSI models with cyclic bending for human coronary atherosclerotic plaque mechanical analysis. J Biomech Eng 131.
17. Teng Z, Tang D, Zheng J, Woodard P, Hoffman A (2009) An experimental study on the ultimate strength of the adventitia and media of human atherosclerotic carotid arteries in circumferential and axial directions. J Biomech 42: 2535-2539.
18. Holzapfel G, Gasser T, Ogden R (2000) A new constitutive framework for arterial wall mechanics and a comparative study of material models. Journal of Elasticity 61: 1-48.
19. Holzapfel G, Gasser T, Stadler M (2002) A structural model for the viscoelastic behavior of arterial walls: Continuum formulation and finite element analysis. European Journal of Mechanics, A/Solids 21: 441-463.
20. Holzapfel G, Sommer G, Gasser C, Regitnig P (2005) Determination of layer-specific mechanical properties of human coronary arteries with nonatherosclerotic intimal thickening and related constitutive modeling. Am J Physiol Heart Circ Physiol 289: H2048-H2058.
21. Valencia AA, Baeza F (2009) Numerical simulation of fluid-structure interaction in stenotic arteries considering two layer nonlinear anisotropic structural model. International Communications in Heat and Mass Transfer 36: 137-142.
22. Li MX, Beech Brandt J, John L, Hoskins P, Easson W (2007) Numerical analysis of pulsatile blood flow and vessel wall mechanics in different degrees of stenoses. J Biomech 40: 3715-3724.
23. Mohammadi H, Bahramian F (2009) Boundary conditions in simulation of stenosed coronary arteries. Cardiovasc Eng 9: 83-91.
24. Hamedani BA, Navidbakhsh M (2011) Blood flow pattern in a coronary bypass with moderate stenosis.
25. Ard, R. ADINA (2008) Theory and Modeling Guide Volume III : ADINA CFD & FSI, volume I. ADINA R & D Inc, Wateron, MA, USA.
26. Cacho F, Doblar M, Holzapfel G (2007) A procedure to simulate coronary artery bypass graft surgery. Med Biol Eng Comput 45: 819-827.
27. Bluestein D, Gutierrez C, Londono M, Schoephoerster R (1999) Vortex shedding in steady flow through a model of an arterial stenosis and its relevance to mural platelet deposition. Ann Biomed Eng 27: 763-773.
28. Nichols WW, O'Rourke MF (2005) McDonald's Blood Flow in Arteries 5Ed: Theoretical, experimental and clinical principles. A Hodder Arnold Publication. Taylor & Francis.